Mon. Not. R. Astron. Soc. **000**, 000–000 (0000) Printed January 21, 2010 (MN LATEX style file v2.2)

High redshift formation and evolution of central massive objects I: model description

B. Devecchi[1], M. Volonteri[2], M. Colpi[3], F. Haardt[1]
[1] *Dipartimento di Fisica & Matematica, Università dell'Insubria, Via Valleggio 11, 22100 Como, Italy*
[2] *Dept. of Astronomy, University of Michigan, Ann Arbor, MI 48109, USA*
[3] *Dipartimento di Fisica G. Occhialini, Università degli Studi di Milano Bicocca, Piazza della Scienza 3, 20126 Milano, Italy*

January 21, 2010

ABSTRACT
Galactic nuclei host central massive objects either in the form of supermassive black holes or nuclear stellar clusters. Recent investigations have shown that both components co-exist in at least a few galaxies. In this paper we explore the possibility of a connection between nuclear star clusters and black holes that establishes at the moment of their formation. We here model the evolution of high redshift discs, hosted in dark matter halos with virial temperatures $> 10^4$ K, whose gas has been polluted with metals just above the critical metallicity for fragmentation. A nuclear cluster forms as a result of a central starburst from gas inflowing from the unstable disc. The nuclear stellar cluster provides a suitable environment for the formation of a black hole seed, ensuing from runaway collisions among the most massive stars. Typical masses for the nuclear stellar clusters at the time of black hole formation ($z \sim 10$) are in the range $10^4 - 10^6$ M$_\odot$ and have half mass radii $\lesssim 0.5$ pc. The black holes forming in these dense, high redshift clusters can have masses in the range $\sim 300 - 2000\,$M$_\odot$.

Key words: black hole physics - instabilities - stellar dynamics - galaxies: nuclei - galaxies:formation - galaxies: star clusters

1 INTRODUCTION

Central massive objects are known to reside in the centers of a large fraction of galaxies either in the form of supermassive black holes (BHs) or nuclear stellar clusters (NCs). Both BHs and NCs have masses that correlate with those of their hosts (Ferrarese et al. 2006; Wenher et al. 2006), suggesting a symbiotic evolution between these nuclear components and the larger structure of their galaxy hosts.

NCs, with masses, $M_{\rm NC}$, ranging between $10^5 - 10^7$ M$_\odot$ (Walcher et al. 2006; Côté et al.(2006); Bokert et al. 2004; Balcells et al. 2007) appear to be more common in galaxies with stellar masses below $\sim 10^{11}$ M$_\odot$, while BHs ($M_{\rm BH} > 10^6$ M$_\odot$) preferentially inhabit galaxies more massive than 10^{10} M$_\odot$ (Ferrarese et al. 2006; Wenher et al. 2006). Despite this apparent dichotomy, a smooth transition exists between NCs and BHs. Some galaxies do host both a NC and an embedded BH (Seth et al. 2008; Graham et al. 2009) and observational estimates seems to indicate mass ratios $M_{\rm BH}/M_{\rm NC} \sim 10^{-4} - 10^{-1}$ (Seth et al. 2008). Interestingly, BHs coexisting with NCs have masses that covers the intermediate range ($10^3 - 10^6$ M$_\odot$) between stellar and supermassive BHs.

Two main scenarios have been proposed to explain the origin of NCs. In the first, NCs are the end product of multiple mergers of globular clusters following their sinking by dynamical friction into the central part of the host galaxy (Tremaine et al. 1975; Capuzzo-Dolcetta & Miocchi 2008; Lotz et al. 2001). In the second, NCs form *in situ* after inflow of gas from the outer part of the host (Milosavljevic 2001): this latter possibility seems more consistent with stellar population studies in NCs (Côté et al.(2006)).

Whereas models of NCs in a cosmological context are still lacking, models of BH seed formation have been developed in the ΛCDM cosmogony. How BH seeds form and how they evolve into the supermassive variety has been the subject of many studies (Begelman & Rees 1986). A natural path to BH formation relies on the first generation of stars (Pop III) born in metal free environments (Madau & Rees 2001; Volonteri et al. 2003). These stars are expected to be more massive than their current counterparts (Abel et al. 2000; Omukai & Palla 2003; Freese et al. 2008; Iocco et al. 2008). PopIII stars that form above a threshold mass of $\simeq 260\,M_\odot$ are believed to directly implode leaving a seed BH of similar mass (Heger et al. 2003). Alternative routes to BH seed formation typically exploit gas-dynamical processes in metal-free galaxies (direct formation models) (Haehnelt & Rees 1993; Loeb & Rasio 1994; Eisenstein & Loeb 1995; Bromm & Loeb 2003; Koushiappas et al. 2004; Begelman, Volonteri & Rees 2006; Lodato & Natarajan 2006). Gravita-

tional instabilities can indeed lead to a vigorous gas inflow into the very central region of protogalactic discs, supplying the necessary matter for the formation of BH seeds.

The above scenarios have a common fundamental ingredient, i.e., the gas hosted in the progenitor halo has not been polluted by metals. Metal pollution marks the end of the formation of PopIII stars and of their seed black holes as fragmentation and formation of low mass stars start as soon as gas is polluted above a critical metallicity threshold, $Z_{\rm crit}$ (Schneider et al. 2006; Bromm et al. 1999, 2002; Omukai et al. 2008; Clark et al. 2008, Santoro & Shull 2006). PopIII stars with masses between 140 and 260 $M_\odot$ are believed to be responsible for starting metal pollution, as they do not leave a relic black hole but explode releasing all metals in the surrounding medium. Star formation is also an impediment for strong gaseous inflows in the center of massive halos as it limits the available mass supply. This does not necessary means the end of the seed formation epoch as a new channel for BH formation opens (Omukai et al. 2008; Devecchi & Volonteri 2009, hereafter DV09).

DV09 showed that the first episode of low-mass, PopII star formation can provide the conditions for the formation of NCs and BH seeds arising in the most compact of these clusters. Gravitationally unstable protogalactic discs whose gas is only mildly polluted by metals, can still produce strong gas inflows into their central regions. Stars start to form in the central few pc where the gaseous mass has been accumulated and the densities are high enough for star formation to set in. Clusters formed in this way are crowded places. Star-star collisions in their core can proceed in a runaway fashion and a very massive star of ~ 1000 $M_\odot$ can build up before the first supernova explodes (Freitag et al. 2006b,a; Portegies Zwart & McMillan 2002; Gurkan et al. 2004). At low metallicities, the final fate of this very massive star is to collape into a BH with mass similar to its progenitor – as mass loss at low metallicity is negligible.

One of the factors that regulate the competition, at a given redshift, between different formation scenarios is the metal enrichment history. Both observational and theoretical works have been performed in order to investigate how metals are distributed as cosmic structures form and evolve (Scannapieco et al. 2003; Tornatore et al. 2006; Savaglio 2006; Savaglio et al. 2005; Prochaska et al. 2003; Prochaska et al. 2007, Kulkarni et al. 2005; Li 2007). These studies have shown that metal enrichment proceeds in a very inhomogeneous fashion. This opens the possibility that different modes of BH seed formation co-exist in different regions of the Universe at the same redshift, instead of being mutually exclusive. As the mean metallicity increases with cosmic time, growing bubbles of polluted gas where the first NCs and their BH seeds form, co-exist with relatively pristine regions where PopIII star formation can still be feasible.

This is the first of a series of papers in which we develop a model aimed at tracing self-consistently metal enrichment, following the hierarchical build-up of halos. We consider metal enrichment and radiative feedback from the first stars together with feedback of successive generations of stars. Our study is applied in the context of BHs and NCs formation in order to determine: (i) if one of the mechanisms outlined above is dominant in the overall seed formation scenario; (ii) if a clear transition in redshift exists between different formation channels or if they co-exist in the same cosmic epoch; (iii) the characteristic redshift at which each process reaches its maximum efficiency; (iv) when the first NCs are expected to form.

In order to address the above questions, we develop in this paper the semi-analytical scheme, aimed at describing the evolution of a single halo in which a central massive object forms. We adopt a ΛCDM cosmology with $\Omega_{\rm b} = 0.041$, $\Omega_{\rm m} = 0.258$, $\Omega_\Lambda = 0.742$, $h = 0.742$ and $n_{\rm s} = 0.963$ as given by five-year WMAP data (Dunkley et al. 2009).

The outline of the paper is as follows. In Section 2 we descibe our recipes for the formation and evolution of a gaseous disc, hosted in a high redshift dark matter halo. In Section 3 we set our model for the formation of NCs resulting from dynamically unstable discs and of BH seeds ensuing from runaway collapse of stars in NCs. In Section 4 we illustrate the results and compare the results of DV09 with those found with our new technique. Finally, in Section 5 we briefly summarise our model.

In the subsequent papers we will apply our semi-analytical code to merger tree histories extracted from the code PINOCCHIO (Monaco et al. 2002a,b). This will allow us to trace halo evolution, keeping track also of their spatial positions, a condition necessary in order to understand the relevance of radiative and SNae feedback.

2 DISC FORMATION

We here consider a dark matter halo of mass $M_{\rm h}$, virialising at redshift $z_{\rm vir}$, assuming that it follows the density profile of an isothermal sphere. Virial radius $R_{\rm vir}$, circular velocity $V_{\rm h}$ and virial temperature $T_{\rm vir}$ are inferred from the top hat collapse model (see for example Barkana & Loeb 2001).

Gas falling into the potential well created by the dark matter is heated by adiabatic compression and shocks, attaining a mean temperature equal to $T_{\rm vir}$. We assign an initial gas mass $(\Omega_{\rm b}/\Omega_{\rm m})\, M_{\rm h}$ and assume that gas follows an isothermal density profile $\rho_{\rm gas}({\rm r})$.

It has been proposed that a critical metallicity $Z_{\rm crit}$ exists above which star formation in the low mass mode starts. We here focus only on those halos whose gas has been enriched above $Z_{\rm crit}$. In the following we describe the details of our treatment for the evolution of halo gaseous component, star formation and BH seed formation.

2.1 Gas cooling

We assume the standard model for disc formation (White & Rees (1978), Cole et al. (2000), Mo, Mao & White 1998). To this purpose for a given $T_{\rm vir}$ and metallicity Z of the gas, the cooling timescale $\tau_{\rm cool}$ can be computed as

$$\tau_{\rm cool} = \frac{3}{2}\frac{\mu m_{\rm H}}{\rho_{\rm gas}(r)}\frac{k_{\rm B}T_{\rm vir}}{\Lambda(T_{\rm vir}, Z)}, \qquad (1)$$

where $\Lambda(T_{\rm vir}, Z)$ is the cooling function. We adopt $\Lambda(T_{\rm vir}, Z)$ tabulated in Sutherland & Dopita (1993). The cooling radius $r_{\rm cool}(t)$ at time t is defined by imposing $\tau_{\rm cool} = t$. Matter inside $r_{\rm cool}$ has time enough to cool down from its initial temperature.

For the disc to form, gas has to both cool down and collapse. The timescale for disc formation will therefore be

the longest between the cooling and the free-fall timescales. In analogy with the computation of $r_{\rm cool}(t)$ we can define a free-fall radius $r_{\rm ff}(t)$ that sets the radius inside which the gas has sufficient time to free-fall into the central structure. During the initial phase of the collapse a mass of cold gas, $M_{\rm cold}$, develops at a rate

$$\dot{M}_{\rm cold} = 4\pi\rho_{\rm gas}(r_{\rm min}(t))r^2_{\rm min}(t)\dot{r}_{\rm min}, \quad (2)$$

where $r_{\rm min} = \min[r_{\rm cool}, r_{\rm ff}]$.

The cold gas is assumed to condense into a rotationally supported disc whose angular momentum $J_{\rm d}$ is a fraction $j_{\rm d}$ of the angular momentum $J_{\rm h}$ of the halo. If the specific angular momentum of baryons is conserved during collapse, $j_{\rm d} = M_{\rm cold}/M_{\rm h}$.

The surface density profile of the disc follows a Mestel, isothermal profile: $\Sigma(R) = \Sigma_0(R_0/R)$ where scale parameters Σ_0 and R_0 are calculated assuming mass and angular momentum conservation (see DV09)[1].

In the following Sections we describe how scale parameters of the disc vary with cosmic time since (i) the disc mass keeps increasing due to the infall of fresh cold gas accreting from the halo (as described by equation 2) and (ii) the gas content changes due to gravitational instabilities that triggers episodes of inflow and star formation (outlined in Section 2.2).

2.2 Gravitational instabilities

The stability of the disc is described in terms of the Toomre parameter Q (Toomre 1964). As the surface density increases since more cold gaseous mass is added to the disc, Q decreases and eventually drops below the critical value for disc stability $Q_{\rm c}$. We here assume $Q_{\rm c} = 2$ (see DV09, Lodato & Natarajan 2007, and Volonteri et al. 2008 for a discussion on $Q_{\rm c}$). At this point the disc develops bar-like structures that can lead to a redistribution of mass and angular momentum.

Inflow of gas driven by gravitational instabilities can be described in terms of an effective viscosity ν. The inflow rate is given by (Lin & Pringle 1987, see also Lodato 2008):

$$\dot{M}_{\rm grav} = 2\pi\nu\Sigma(R)|\frac{{\rm dln}\Omega(R)}{{\rm dln}R}|, \quad (3)$$

where Ω is the angular velocity and

$$\nu = \eta\left(\frac{Q_c^2}{Q^2} - 1\right)\frac{c_s^3}{\pi G\Sigma(R)}. \quad (4)$$

We set in our reference model $\eta = 0.3$ (Gammie 2001) but we also compare our result with simulations run with $\eta = 1$ (high efficiency inflow) and $\eta = 0.1$ (low efficiency inflow). The sound speed $c_{\rm s}$ corresponds to a gas with temperature of 8000 K[2].

The inflow rate that channels mass in the central region of the disc is then:

$$\begin{aligned}\dot{M}_{\rm grav} &= \frac{2\eta c_s^3}{G}\left[\left(\frac{Q_{\rm c}}{Q}\right)^2 - 1\right] = \\ &= \frac{\eta c_{\rm s}}{GV_{\rm h}^2}\left[\pi^2G^2Q_c^2\Sigma_0^2R_0^2 - 2c_s^2V_{\rm h}^2\right]. \quad (5)\end{aligned}$$

Following DV09 we assume that the inner surface density profile changes its scaling with radius as $\propto R^{-5/3}$, according to simulations by Mineshige & Umemura (1999). The transition radius, $R_{\rm tr}$, between the two profiles is given by:

$$R_{\rm tr} = \frac{M_{\rm inf}}{4\pi\Sigma_0R_0}, \quad (6)$$

where $M_{\rm inf}$ is the net mass inflowing from the outer disc ($R > R_{\rm tr}$, see DV09 and equation 9).

For a given set of $M_{\rm h}$, $T_{\rm gas}$ and $Q_{\rm c}$, a maximum angular momentum exists below which a disc becomes unstable $\lambda < 1/8\Omega_b/\Omega_m Q_c\sqrt{T_{\rm vir}/T_{\rm gas}}$ where $T_{\rm gas}$ is temperature of the cold gaseous disc. Discs with higher rotation are more stable agains fragmentation as the amount of mass that needs to be removed from the Mestel disc in order to reach $Q = Q_{\rm c}$ is lower. The inflow mass decreases for halos with large spin parameters.

2.3 Star formation

If the disc grows strongly unstable, star formation sets in, consuming part of the gas that would otherwise flow into the central region. Further evolution of $M_{\rm inf}$ is then regulated by the competition between star formation in the outer Mestel disc and funneling of gas in its center.

An unstable disc starts fragmenting into bound clumps once the gravitationally induced stress exceeds a critical value corresponding to $\dot{M}_{\rm crit} = 0.06\,c_s^3/G$ (Lodato & Natarajan 2007). We allow fragmentation in the Mestel disc only in those regions where the coolign rate Λ exceeds the adiabatic heating rate (see the discussion in DV09). This condition determines the location of a radius $R_{\rm SF}$ where stars are allowed to form.

We denote the time lag between cloud formation and collapse to form stars as $t_{\rm lag}$. This is basically the lifetime of molecular clouds; in our model it corresponds to the delay between the onset of instability (that we assume to be the driver leading to the formation of the clouds) and the start of the star formation event. Observational estimates for lag times range from 1 to 7 Myrs (Klessen et al. 2009). We assume $t_{\rm lag} = 3.5$ Myr. We have checked that our results are not strongly affected by the assumed value of $t_{\rm lag}$: final

[1] Note that the evolution of the collapsing structure and the initial assembly of the disc is described in a way similar to DV09. The main difference is that the assembly of the disc is here followed solving esplicitly for the time evolution of the cold gas, instead of assuming that a fixed fraction of the halo gas cools down instantaneously.

[2] In this paper we consider only halos illuminated by a flux in the Lyman-Werner (LW) band (11.2-13.6 eV). LW photons can photo-dissociate H_2 molecules, thus suppressing cooling below 8000 K, as dictated by Lyα cooling. Gas could in principle cool down to much lower temperature in presence of H_2. Less massive, colder discs form, leading to a much lower inflow. This prevents the formation of BH seeds unless higher inflow efficiencies are considered. We will consider this more general case in our next paper, where LW flux ensuing from star formation history in a cosmological context will be calculated.

black hole seed masses change by a factor 2-3 for $t_{\rm lag}$ ranging between 1 and 7 Myrs.

We assume a star formation rate surface density $\Sigma_{\rm SFR}$ that follows the empirical Schmidt-Kennicutt law (Kennicutt 1998):

$$\Sigma_{\rm SFR} = 2.5 \cdot 10^{-4} \left(\frac{\Sigma(R)}{1\,{\rm M_\odot pc^{-2}}} \right)^{1.4} {\rm M_\odot yr^{-1} kpc^{-2}}, \quad (7)$$

and calculate the star formation rate $\dot{M}_{*,\rm d}$ by integrating over the region of the disc where stars form. We thus integrate $\Sigma_{\rm SFR}$ between $R_{\rm tr}$ and $R_{\rm SF}$ to infer a star formation rate $\dot{M}_{*,\rm d}$ in the outer disc:

$$\dot{M}_{*,\rm d} = 5\pi \times 10^{-4} \left[\Sigma_0 R_0\right]^{7/5} (R_{\rm SF}^{3/5} - R_{\rm tr}^{3/5}). \quad (8)$$

Star formation decreases the amount of gas that can be funnelled in the inner disc. For this reason and as long as $\dot{M}_{\rm grav} > \dot{M}_{\rm crit}$ we assume a net inflow rate $\dot{M}_{\rm inf}$ equal to

$$\dot{M}_{\rm inf} = \dot{M}_{\rm grav} - \dot{M}_{*,\rm d}. \quad (9)$$

2.4 Supernova feedback

Approximately 3 Myrs after an episode of star formation, the most massive stars explode as SNae. Metals processed in their centers are released into the surrounding gas, increasing the metal content. Metal yields and energy production depend on the initial mass function (IMF) of the stars. We here assume a Salpeter IMF with minimum ($M_{\rm l}$) and maximum ($M_{\rm u}$) mass of 0.1 and 100 $\rm M_\odot$ respectively normalized to 1 $\rm M_\odot$.

We correlate the rate of metal production with the star formation rate in the disc assuming that the total mass in metals scales as:

$$\dot{M}_{\rm met} = Y_{\rm met} \nu_{\rm SN} \dot{M}_*, \quad (10)$$

where $Y_{\rm met}$ is the total IMF-averaged metal yield and $\nu_{\rm SN}$ is the fractional number of SNae exploding after the formation of a mass M_* in stars. We assume that SN progenitors are stars with masses between 10-50 $\rm M_\odot$ (Scannapieco et al. 2003)[3]. With our prescriptions $Y_{\rm met} = 1.6\,\rm M_\odot$ and $\nu_{\rm SN} = 0.00484$.

SN explosions in high redshift halos can be extremely destructive. SN driven bubbles can push away part of the gas in the halo, eventually fully depriving the host of its gas. The efficiency of gas depletion depends on the depth of the potential well of the host and on the energy released during the explosion.

Using energy conservation we compute the amount of mass that is removed from the disc plus halo as a result of SN esplosions, assuming that each single explosion releases an energy $E_{\rm SN} = 10^{51}$ erg (Woosley & Weaver 1995). The resulting outflow rate $\dot{M}_{\rm sh}$ is

$$\dot{M}_{\rm sh} = \frac{f_w \nu_{\rm SN} E_{\rm SN} \dot{M}_*}{2\,(1+\Omega_{\rm b}/\Omega_{\rm m})\,G M_{\rm h}/R_{\rm vir} + \frac{1}{2} v_{\rm sh}^2}, \quad (11)$$

where f_w is the fraction of energy channelled into the outflow, $v_{\rm sh}$ is the velocity of the outflow at the virial radius. We refer the reader to Appendix A for details of our recipes for gas depletion. Lastly, we define the retention fraction coefficient $f_{\rm ret} \equiv (M_{\rm gas} - M_{\rm sh})/M_{\rm gas}$. After the explosion we assume that a fraction $f_{\rm ret}$ of the metals yields produced remains in the host.

2.5 Disc evolution

The evolution of an unstable disc is followed tracing the time dependence of $M_{\rm cold}$, $M_{\rm inf}$, $M_{*,\rm d}$ and $M_{\rm sh}$, integrating equations 2, 8, 9 and 11 assuming that initially all the gaseous mass is hot ($T = T_{\rm vir}$).

Changes in these quantities over cosmic time correspond to changes in the scale parameters of the Mestel disc (Σ_0, R_0) and $R_{\rm tr}$. Angular momentum conservation and total mass conservation in the system are imposed to infer the following equations linking the current values of $\Sigma_0(t)$ and $R_0(t)$ to their value at the moment in which the disc reaches the instability regime:

$$\Sigma_0(t) = \Sigma_0(0) \left[1 - \frac{m_{\rm a}(t)}{m_{\rm d}(t)}\right]^3, \quad (12)$$

$$R_0(t) = R_0(0) \left[1 - \frac{m_{\rm a}(t)}{m_{\rm d}(t)}\right]^{-1} \quad (13)$$

where $m_{\rm d}(t) = M_{\rm cool}(t)/M_{\rm h}$ and $m_{\rm a}(t)$ is the total fractional gaseous mass removed from the outer disc, either via star formation, inflow and outflows from SNae. The disc alternates episodes of instability to states of quiescence: as Q increases above $Q_{\rm c}$, the instability is quenched. Disc parameters evolve regulated by the amount of new mass that is added by accretion from the halo.

We halt the simulations as soon as the hot halo gas is consumed and the disc is in a stable state. We proceed on studying in the next section the evolution of the gas that has been funnelled at the center of the disc where we expect that a NC and/or a BH seed form.

3 CENTRAL MASSIVE OBJECT FORMATION

In the previous Section we focused on the evolution of Toomre unstable discs. Here we study the formation of a NC from a mass reservoir $M_{\rm inf}$, funnelled into $R_{\rm tr}$ after $t_{\rm lag}$.

Star formation in the central part of the disc can proceed with a higher efficiency with respect to the outer disc as higher pressure and density are expected there (Elmegreen & Efremov 1997, Li et al. 2007). We assume that a fraction $\epsilon_{\rm SF}$ of $M_{\rm inf}$ is converted into stars and we here adopt $\epsilon_{\rm SF} = 1$ (Li et al. 2007). The mass and radius of the cluster are $M_{\rm cl} = \epsilon_{\rm SF} M_{\rm inf}$ and $R_{\rm cl} = \min(R_{\rm SF}, R_{\rm tr})$.

NCs formed in this way are very compact and unstable objects. Numerical studies of stellar clusters have shown that gravitational encounters between stars can drive the clusters

[3] We here follow Tsujimoto et al 1995 and assume that stars with masses greater than 50 $\rm M_\odot$ collapse into a BH without ejecting heavy metals.

towards core collapse, leading to a contraction of the core where physical collisions between stars are frequent[4]. Core collapse is driven by dynamical friction of the more massive stars. Star-star collisions between massive stars in the cluster core can happen in a runaway fashion, leading to the build up of a very massive star (VMS), whose mass can be as high as 1000 $M_\odot$ (Portegies Zwart et al. 1999,2004; Freitag et al. 2006a,b; Gurkan et al. 2004).

After ~ 3 Myrs the first SNae explode. For the systems we are interested in, this happens before the inflow process ends. We assume that a NC is able to produce a BH seed only if it undergoes core collapse before the first SN explosion. We compute the mass of the nuclear star cluster, $M_{\rm cl,0}$, 3 Myr after the onset of star formation, and from these we infer the core collapse timescale, $t_{\rm cc}$. For those systems with $t_{\rm cc} \leqslant 3$ Myr, we calculate the mass for the very massive star $M_{\rm VMS}$ as in DV09:

$$M_{\rm VMS} = m_* + 4 \times 10^{-3} M_{\rm cl} f_c \ln \lambda_C \ln \left(\frac{3{\rm Myr}}{t_{\rm cc}} \right), \qquad (14)$$

where $f_{\rm c} = 0.2$ and $\ln \lambda_C = \log(0.1 M_{\rm cl,0}/\langle m \rangle)$ (Portegies Zwart & McMillan (2002)).

At low metallicities, stars more massive than 260 $M_\odot$ are expected to leave a remnant BH, that retains most of its progenitor mass. Each time $M_{\rm VMS}$ is greater than 260 $M_\odot$ we assume a BH seed is formed with $M_{\rm BH} = M_{\rm VMS}$. For a BH seed to form the stellar cluster needs a total mass $\geqslant$ 260 $M_\odot$ in massive stars that can segregate. We here assume that stars more massive than 10 $M_\odot$ efficiently segregate in the cluster core. Once all these more massive stars are consumed collisions are assumed to stop. For our chosen IMF a minimum VMS mass of 260 $M_\odot$, corresponds to a minimum cluster mass of 1.5×10^4 $M_\odot$. We here include this caveat and assume that BH seeds can form only in those nuclear clusters more massive than this threshold.

The ability of runaway collisions to form an intermediate mass BH also depends on the metallicity of the gas from which the stars originated. Recent simulations of star-star collisions have shown that at metallicities higher than $10^{-3}\, Z_\odot$, physical collisions are too disruptive, and the build up of a star with mass greater than 260 $M_\odot$ is inhibited (Glebbeek et al. 2009). For this reason we assume that a BH seed forms only at metallicities $< 10^{-3}\, Z_\odot$.

Summarising, BHs form provided that the following conditions are met: (i) $Z > Z_{\rm crit}$ so that a NC can form; (ii) λ is sufficiently small for the disc to reach gravitational instability; (iii) clusters form with $t_{\rm cc} < 3$ Myr and (iv) massive enough to host an adequate amount of stars with $m_* > 10$ $M_\odot$.

[4] Note that these studies concentrate on halo stellar clusters. NC dynamics can be alterated with respect to their halo conterparts by (i) the presence of the external stellar environment and (ii) continuos gas accretion. These two effects work on opposite directions: cluster contraction can be reverted as stars of the more rarefied outer-system are trapped into the central clusters. Inflow of gas can instead drive an acceleration of core collapse as it deepens the potential well. The final outcome resulting from the competition between them is not easy to infer and it is behind the aim of this paper. We will address this issue in a follow-up paper.

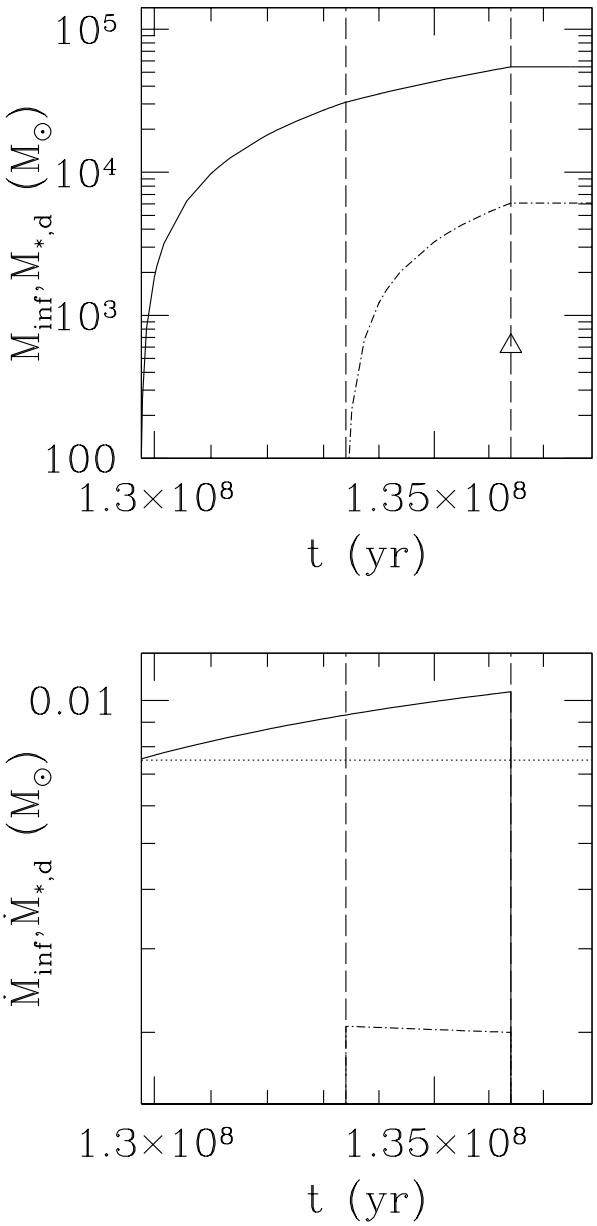

Figure 1. Upper panel: $M_{\rm inf}$ (solid line) and $M_{*,\rm d}$ (dash-dotted lines) versus time t for our reference models. The triangle highlights the BH mass at the moment of its formation. Lower panel: $\dot{M}_{\rm inf}$ (solid line) and $\dot{M}_{*,\rm d}$ (dash-dotted line) for our reference model as a function of time. The horizontal dotted line marks the critical threshold for fragmentation $\dot{M}_{\rm crit}$. Vertical lines define the different evolutionary phases of the disc properties as described in the text.

4 RESULTS

In this Section we describe how disc properties are shaped by gravitational instabilities and star formation. Our reference halo has mass $M_{\rm h} = 6.5 \times 10^7$ $M_\odot$, and forms at $z_{\rm vir} = 10$: we further adopt $\lambda = 0.05$, $Z/Z_\odot = 10^{-4}$, $\eta = 0.3$, $Q_{\rm c} = 2$, $\epsilon_{\rm SF} = 1$ and $t_{\rm lag} = 3.5$ Myr.

4.1 Disc and cluster properties

In this subsection we illustrate the evolution of the reference disc model. After a time $\tau_{\rm inst} = 1.3 \times 10^8$ yr, the disc has grown enought to hit the instability threshold as it has assembled enough mass so that the Toomre parameter drops below $Q_{\rm c}$. The upper (lower) panel in Fig. 1 shows $M_{\rm inf}$ ($\dot{M}_{\rm inf}$) and $M_{*,\rm d}$ ($\dot{M}_{*,\rm d}$) as a function of time t, from the time the disc becomes unstable until the time of formation of the central BH. The evolution proceeds along different phases:

1) $\tau_{\rm inst} < t < \tau_{\rm inst} + t_{\rm lag}$: at $t = \tau_{\rm inst}$ the disc starts collecting gas into the center and this leads to an enhancement of $M_{\rm inf}$. The disc parameters are such that $\dot{M}_{\rm grav}$ is greater than $\dot{M}_{\rm crit}$ (horizontal dotted line in the righ panel of the Figure). Clump formation in the disc sets in but these newly formed clouds have not had enough time to collapse until a time $t_{\rm lag}$ has elapsed.

2) $\tau_{\rm inst} + t_{\rm lag} < t < \tau_{\rm inst} + t_{\rm lag} + 3\,$Myr: star formation begins. The critical density for star formation remains constant as metals have not been released yet and the star formation radius still remains close to its initial value. Both $M_{\rm inf}$ and $M_{*,\rm d}$ increase until the first SNae explode. We label the nuclear mass at this time as $M_{\rm cl,0}$.

3) $t > \tau_{\rm inst} + t_{\rm lag} + 3\,$Myr: the first SNae explode affecting the subsequent evolution of the system. Part of the metals produced in stars are released in the surrounding gas increasing the metallicity above $Z_{\rm crit}$. At the same time SN explosions evacuate gas from the system lowering the surface density. As a result the Toomre parameters increases above $Q_{\rm c}$.

The disc then lingers on a marginally stable configuration thanks to the high $\dot{M}_{\rm sh}$ that is able to counter-balance $\dot{M}_{\rm cool}$. Fragmentation in the disc is temporary halted as $\dot{M}_{\rm grav}$ drops below $\dot{M}_{\rm crit}$. At later times, the surface density starts to increase again, as hot gas in the halo continues to cool. The disc then enter a new cycle of instability, and evolution terminates when the hot gas reservoir has been consumed.

4.2 Dependence on input parameters

We here explore disc evolution as a function of the halo mass, $M_{\rm h}$, for three different values of inflow efficiency, η, and as a function of the initial metallicity Z.

Fig. 2 shows the NC mass $M_{\rm cl,0}$ (solid lines) and BH mass $M_{\rm BH}$ (log dashed lines) at the time of BH formation, and the stellar disc mass $M_{*,\rm d}$ (dash-dotted lines), and net inflow mass $M_{\rm inf}$ (dotted lines) at the end of the simulation, as a function of $M_{\rm h}$, for different values of η.

The NC mass, $M_{\rm cl,0}$, depends weakly on the host mass, $M_{\rm h}$, and somewhat more strongly on the inflow efficiency, η. By contrast, the final stellar disc mass depends significantly on $M_{\rm h}$. This is because (i) more massive halos have a larger gas mass and retention efficiency ($f_{\rm ret}$); (ii) gas cools more rapidly in larger halos. This allows for a larger departure of the Toomre parameter Q from $Q_{\rm c}$, and larger inflow ($\dot{M}_{\rm grav}$, see equation 5). $\dot{M}_{\rm grav}$ is larger than the critical inflow triggering fragmentation, $\dot{M}_{\rm crit}$, and more stars form in the outer disc. For $\eta = 0.1$ a threshold in $M_{\rm h}$ exists below which $\dot{M}_{\rm grav} < \dot{M}_{\rm crit}$ always, and $M_{*,\rm d}$ drops to zero.

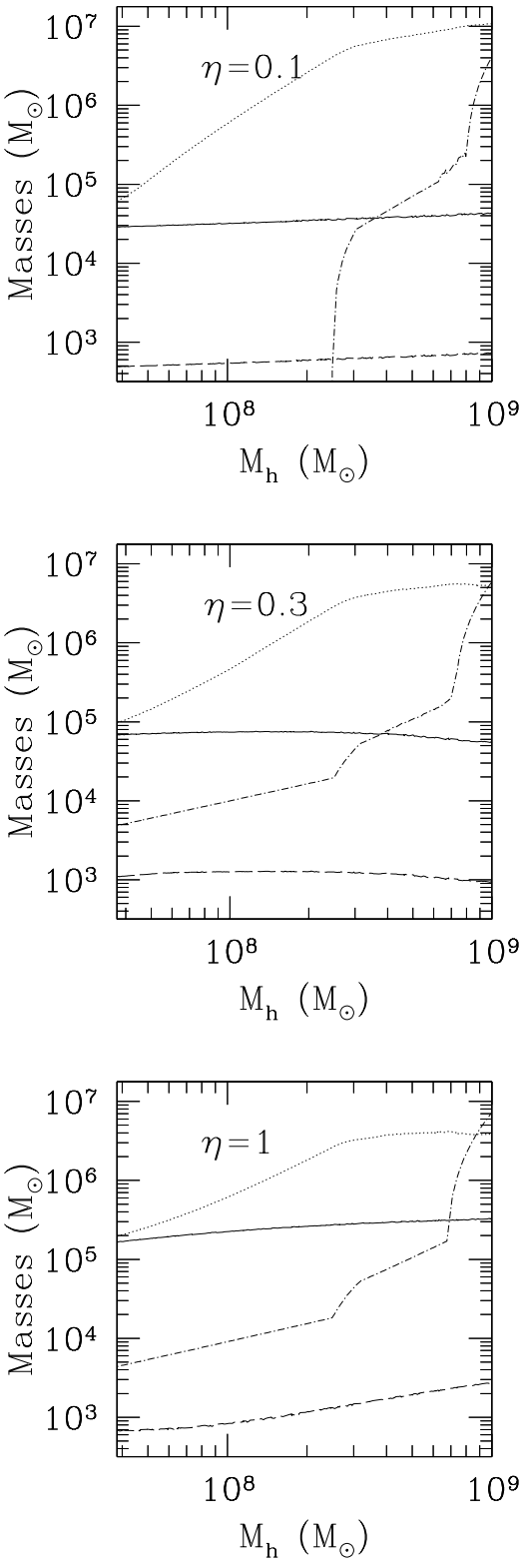

Figure 2. Mass $M_{\rm cl,0}$ (solid lines) of the NC and $M_{\rm BH}$ (dashed lines) at the time the BH forms, and $M_{\rm inf}$ (dotted lines), $M_{*,\rm d}$ (dash-dotted lines) at the end of the simulations, as a function of $M_{\rm h}$ for different inflow efficiencies. High, central and low panels refer to $\eta = 0.1$, 0.3 and 1, respectively. Reference properties for the halo are $z_{\rm vir} = 10$ and $\lambda = 0.05$; for the baryonic component $Z/Z_\odot = 10^{-4}$, $Q_{\rm c} = 2$ and $\epsilon_{\rm SF} = 1$.

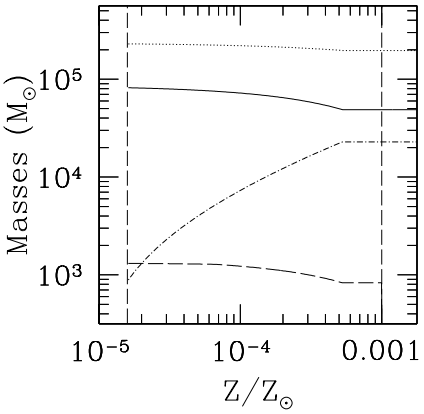

Figure 3. $M_{\rm cl,0}$ (solid lines), $M_{\rm BH}$ (dashed lines), $M_{\rm inf}$ (dotted lines) and $M_{*,\rm d}$ (dash-dotted lines) as a function of the initial metallicity of the gas for our reference halo. The halo mass is kept constant at its reference value $M_{\rm h} = 6.7 \times 10^7$ M$_\odot$. Vertical lines mark the minimum metallicity for low-mass star formation, $Z_{\rm crit} \simeq 10^{-4.87}\, Z_\odot$, and the maximum metallicity that allows BH formation, $Z_{\rm crit} \simeq 10^{-3}\, Z_\odot$.

Dotted lines in Fig. 2 show the net inflow mass, $M_{\rm inf}$, at the end of the simulations. $M_{\rm inf}$ increases with increasing $M_{\rm h}$ as a result of both initially larger gas masses and deeper potential wells. $M_{\rm inf}$ depends weakly on η. For higher η more gas is consumed by extended star formation before it can reach the nucleus and final $M_{\rm inf}$ are lower.

Disc evolution depends also on the initial metallicity Z. The metallicity determines when stars can form and it is thus a key parameter: there is a minimum metallicity where 'normal' stars star forming, $Z_{\rm crit} \simeq 10^{-4.87}\, Z_\odot$, and a maximum metallicity that allows BH formation, $Z_{\rm crit} \simeq 10^{-3}\, Z_\odot$.

In Fig. 3, the NC mass $M_{\rm cl,0}$ (solid line), BH mass $M_{\rm BH}$ (dashed line), net inflow mass $M_{\rm inf}$ (dotted line), and stellar disc mass $M_{*,\rm d}$ (dash-dotted line) are plotted as a function of the initial gas metallicity. Star formation sets in only for $Z > Z_{\rm crit}$ (left vertical dashed line in Fig. 3). For the majority of the systems we are considering here, $R_{\rm SF} > R_{\rm tr}$. The first three quantities are almost independent of metallicity, as long as Z is in the range between the minimum and maximum value. The disc stellar mass is instead very sensitive to the exact value of the metallicity. $M_{*,\rm d}$ increases with Z (see equation 8). Mass is consumed instead of flowing into the nucleus, and $M_{\rm cl,0}$ weakly decreases[5]. When the metallicity is large enough that $R_{\rm SF}$ equals R_0 than the whole disc forms stars, and the dependence on Z disappears.

In our reference model we set $\lambda = 0.05$. The distribution of spin parameters can be described as a log-normal distribution with peak at $\lambda \sim 0.03 - 0.05$ and dispersion ~ 0.5. For our reference halo the maximum λ allowing for instability is 0.07. Approximately 96% of the halos in the interesting mass range have $\lambda < \lambda_{\rm max}$ and are therefore prone to disc instabilities.

If $Q_{\rm c}$ is lowered to unity, instabilities are easily quenched, and the process becomes less efficient (see upper right panel in Fig. 4).

4.3 NC and BH masses versus redshift

In this Section we apply our prescriptions for the cooling of gas, star formation and inflow to determine the properties of the NC and BH populations, in low metallicity environments.

To this purpose, we construct a sample of halos with the same properties of those analysed in DV09. We focus on halos with $z_{\rm vir}$ ranging between 5 and 30 corresponding to $T_{\rm vir}$ between 10^4 K and 1.8×10^4 K (Barkana & Loeb 2001), and we determine their frequency using a modified version of the Press & Schechter formalism (Sheth & Tormen 1999) in a WMAP5 cosmology (Dunkley et al. 2009). To each halo, we assign a value of the spin parameter, λ, extracted from the probability distribution found in the Millennium simulations. We here adopt the same prescriptions for the metallicity evolution as in model A in DV09, while we adopt the model described in this paper for the evolution of each disc-halo. The model is thus an improvement of that discussed in DV09. More realistic models that follow metal enrichment self-consistently will be described in Paper II. We consider different inflow efficiencies η=1 (dotted lines), 0.3 (solid lines) and 0.1 (short-dashed lines) for $Q_{\rm c} = 2$ and $\eta = 0.3$ for $Q_{\rm c}$=1 (long-dashed lines).

In the upper left panel of Fig. 4 we show the evolution of the NC mass, $\langle M_{\rm cl,0} \rangle$ (averaged over the sample) as a function of redshift. NCs start to form at $z = 14$, as halos are polluted above the critical metallicity for fragmentation (see DV09)[6]. BH seeds start to form after the formation of the first NCs. In the upper right panel of Fig. 4 we compute the fraction $f_{\rm BH}$ of halos with $T_{\rm vir} > 10^4$ K hosting a BH seed, as a function of redshift. $f_{\rm BH}$ is regulated by the fraction of halos with $Z_{\rm crit} < Z < 10^{-3}\, Z_\odot$: it first increases as more and more halos are polluted, and then decreases when most halos reach $Z = 10^{-3} Z_\odot$. $f_{\rm BH}$ in this paper are larger than those found in DV09 (see their Figure 8, upper panel) by a factor 10. With the prescriptions we adopt here, $M_{\rm cool}$ evolves with time, regulated by cooling of the halo gas whereas in DV09 a fixed $M_{\rm cool}/M_{\rm h}$ is used. This implies that for a given $Q_{\rm c}$, the fraction of unstable discs that form is increased.

Mean black hole masses $\langle M_{\rm BH} \rangle$ versus redshift z are plotted in Fig. 4 (lower left panel). $\langle M_{\rm BH} \rangle$ spans values between a few hundred M$_\odot$ and 2000 M$_\odot$. For most of the NCs considered here, the growth of the VMSs is limited by the amount of stars with $m_* > 10$ M$_\odot$. Lower $\langle M_{\rm cl,0} \rangle$ thus lead to lower mass seed BHs. An exception occurs for the

[5] Note that for systems with $R_{\rm SF} < R_{\rm tr}$, the initial cluster mass, $M_{\rm cl,0}$, increases with Z as (i) extended star formation is not allowed in the outer disc, so that the amount of mass funnelled into the nucleus remains constant; (ii) higher metallicities correspond to higher $R_{\rm SF}$ so that to a larger amount of nuclear gas can be converted into stars. This case was considered in DV09, we refer to that work for a discussion of this regime.

[6] In our reference model ($\eta = 0.3$, $Q_{\rm c} = 2$) the mean cluster mass $\langle M_{\rm cl,0} \rangle$ decreases with redshift as the metallicity increases. This behaviour appears only as the majority of the systems we are considering here have $R_{\rm SF} > R_{\rm tr}$ (that is, stars form in most of the disc). If this were not the case, the behaviour of $\langle M_{\rm cl,0} \rangle$ versus redshift would be the opposite (see DV09).

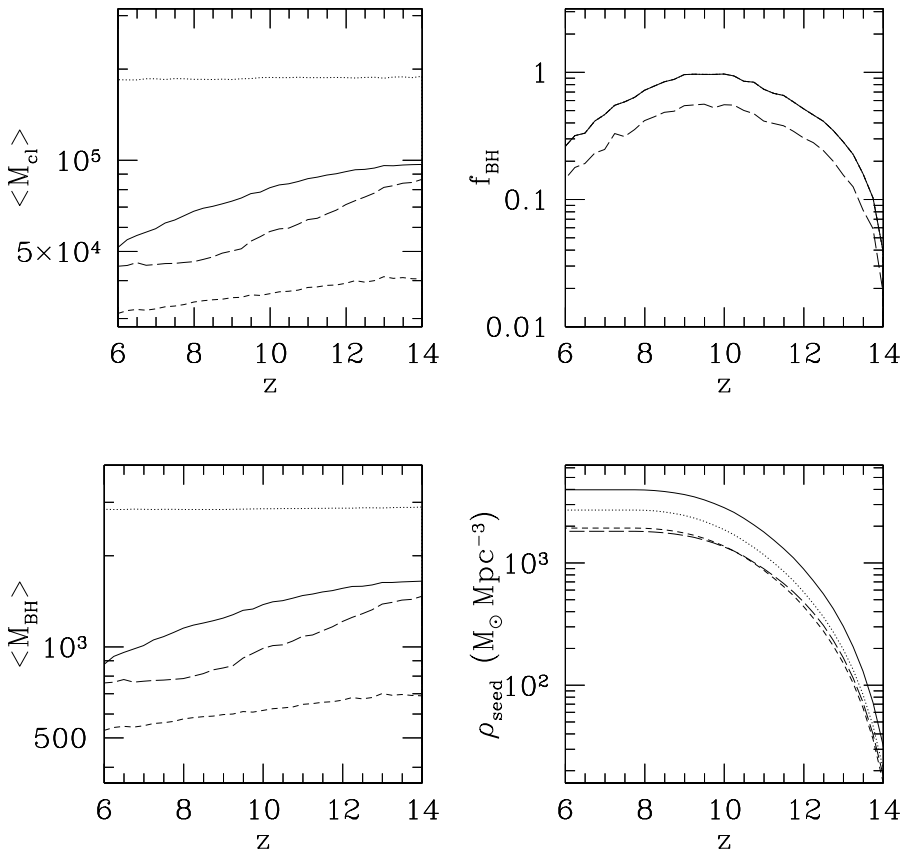

Figure 4. Panels from up to low: $\langle M_{\rm cl,0}\rangle$ (for those clusters able to form a seed BH), $f_{\rm BH}$, $\langle M_{\rm BH}\rangle$ and $\rho_{\rm seed}$ as a function of redshift for different values of η and $Q_{\rm c}$. Line styles: solid lines refer to a model with $\eta = 0.3$, $Q_{\rm c} = 2$, dotted lines refer to a model with $\eta = 1$, $Q_{\rm c} = 2$, short-dashed lines refer to a model with $\eta = 0.1$, $Q_{\rm c} = 2$, long-dashed lines refer to a model with $\eta = 0.3$, $Q_{\rm c} = 1$.

highest $M_{\rm cl,0}$ (i.e. $\eta = 1$): for these systems $t_{\rm cc}$ is long and not all massive stars contribute in building up the VMS. $\langle M_{\rm BH}\rangle$ stays at a near constant value ~ 900 M$_\odot$, at any redshift.

Comoving BH seed densities are plotted in the lower right panel. $\rho_{\rm seed}$ depends on both BH formation efficiencies and masses attained. They are found to depend weakly on the parameters: final $\rho_{\rm seed}$ only differs of a factor 2, ranging between 2000 and 4000 M$_\odot$ Mpc^{-3}.

5 SUMMARY

In this paper, the first of a series, we presented a model for the formation of high redshift, metal poor NCs and their embedded BH seeds. The channel that we propose can be summarized as follows:

- After the virialisation of the halo, hot gas cools down and the presence of angular momentum leads to the formation of a cold gaseous disc. The disc accretes gas from the halo and grows in mass, increasing its surface density to the extent that gravitational instabilities develop. This leads to the growth of non-axisymmetric perturbations that redistribute angular momentum, driving mass into the central part of the halo.
- For those systems where the metallicity Z exceedes $Z_{\rm crit}$ and $\dot{M}_{\rm grav} > \dot{M}_{\rm crit}$, star formation in the extended disc can set in, consuming part of the mass that would otherwise been accreted in the center. The inner density profile steepens inside a transition radius where a compact nuclear stellar cluster forms.
- In those NCs where $t_{\rm cc} < 3$ Myr, core collapse anticipates stellar evolution and runaway collisions between the most massive stars build up a very massive star that finally implodes leaving a remnant BH seed.
- The evolution continues and it is driven by the competition between star formation, triggered by prolonged cooling of hot halo gas and SN explosions that evacuate part of it.
- Evolution halts as soon as the hot halo gas is consumed/blown away and the disc settles into a state of stationary equilibrium.

We apply our recipes to a set of halos with $T_{\rm vir} > 10^4$ and properties typical of z ∼10-20. We determine how changing halo properties and model parameters influence the final NC and BH seed population. The NCs have masses, at the moment of BH formation, of $10^4 - 10^6$ M$_\odot$ and host BHs with masses between 300 and a few 10^3 M$_\odot$.

We compared our new prescriptions with the results of DV09. The mean NC masses are found to decrease with

decreasing redshift: higher metallicities usually correspond to larger star formation rates in the extended disc. These reduce the amount of gas channelled into the center, leading to less massive clusters. Except for the more massive NCs, $M_{\rm BH}$ is dictated by the availability of massive stars. The decrease in $M_{\rm cl,0}$ consequently leads to less massive black holes. The total mass densities in BH seeds, $\rho_{\rm seed}$, are higher with respect to DV09 as a result of the larger number of gravitationally unstable discs. In our model we do not take into account any BH growth by accretion, nor their assembly during galaxy clustering. Comoving densities found here are thus lower limits.

In the second paper of this series we will apply this semi-analytical scheme to merger tree histories to trace NC and BH seed formation into a cosmological context. In the third, we will follow the evolution of the emerging BH population through accretion and clustering and compare our results with current observation of BH occupation frequency in low redshift galaxies, quasar luminosity functions, etc.

APPENDIX A: GAS DEPLETION FROM SN FEEDBACK

In this section we describe the prescription used to infer the amount of mass lost from the host following a SN episode. Under the assumption that the gas follows an isothermal profile

$$\rho_{\rm gas} = \frac{\Omega_{\rm b}}{\Omega_{\rm m}} \frac{V_{\rm h}^2}{4\pi G r^2}, \tag{A1}$$

we compute the initial binding energy of the system $E_{\rm b,in}$ inclusive of the dark matter and gaseous component[7].

$$E_{\rm b,in} = -\frac{GM_{\rm h}^2}{R_{\rm vir}} \left(1 + \frac{\Omega_{\rm b}}{\Omega_{\rm m}}\right)^2. \tag{A2}$$

After removing a gaseous mass $M_{\rm sh}$ the new binding $E_{\rm b,f}$ is

$$E_{\rm b,f} = -\frac{GM_{\rm h}^2}{R_{\rm vir}} \left(1 + \frac{\Omega_{\rm b}}{\Omega_{\rm m}} - \frac{M_{\rm sh}}{M_{\rm h}}\right)^2. \tag{A3}$$

Energy conservation imposes the following equality: $E_{\rm b,in} + \mathcal{E}_{\rm SN} = E_{\rm b,f} + K_{\rm SN}$, where $\mathcal{E}_{\rm SN}$ is the energy injected by the SN explosions and $K_{\rm SN}$ is the kinetic energy of the outflow that is leaving the halo .

The energy $\mathcal{E}_{\rm SN}$ by SNae, over a time t, is given by

$$\mathcal{E}_{\rm SN}(t) = \nu_{\rm SN} E_{\rm SN} \int_0^t \dot{M}_* {\rm d}s \tag{A4}$$

where $E_{\rm SN}$ is the energy of a single SN explosion, set equal to 10^{51} erg, $\dot{M}_* = \epsilon_{\rm SF}\dot{M}_{\rm inf} + \dot{M}_{*,\rm d}$ and $\nu_{\rm SN}$ is the ratio between the total number of SNae exploding after the formation of a mass M_* of stars, divided by M_*. SNae start to explode after 3 Myr from the onset of the star formation episode. We assume that at that time all stars with masses in the SN regime explode together giving rise to a single bubble and that a fraction f_w of the total energy released by SN explosions, is channeled into the outflow. Following Scannapieco et al. (2003), we relate f_w with the halo mass as follows. We define $\delta_{\rm B}(M_{\rm h})$ as

$$\delta_{\rm B}(M) = \begin{cases} 1.0, & \tilde{N}_{\rm t} \leqslant 1 \\ 1.0 - 0.165\ln(\tilde{N}_{\rm t}^{-1}), & 1 \leqslant \tilde{N}_{\rm t} \leqslant 100 \\ \left[1.0 - 0.165\ln(100)\right] 100\tilde{N}_{\rm t}^{-1} & 100 \leqslant \tilde{N}_{\rm t} \end{cases} \tag{A5}$$

where $\tilde{N}_{\rm t} \equiv 1.7\times10^{-7}(\Omega_{\rm b}/\Omega_{\rm m})M_{\rm h}/\,{\rm M}_\odot$. f_w is then given by $f_w = \delta_{\rm B}(M_{\rm h})/\delta_{\rm B}(M_{\rm h} = 2\times10^8\,{\rm M}_\odot)$. This prescription follows from the scaling relation found in Ferrara et al. (2000), normalised with the result found by Mori et al. (2002).

Let us now compute $K_{\rm SN} \equiv 1/2 M_{\rm sh} v_{\rm sh}^2$. Here the shell velocity is calculated at the moment it reaches $R_{\rm vir}$. The topology of early metal enrichment can be extremely complex. Enriched gas first propagates into the cavities created by the shock (Greif et al. 2007), and after the bubble shell leaves the host, it spreads mainly into voids, leading to a very anisotropic spatial distribution of metals. We here neglect these degrees of complexity and simply assume that SN-driven bubbles evolve in spherical symmetry. The shell radius is assumed to follow the Sedov-Taylor solution, as long as the pressure of the bubble drops below the value of the surrounding medium. The shell radius $R_{\rm sh}$ evolves with time t as

$$R_{\rm sh} = 1.15 \left(\frac{f_w \mathcal{E}_{\rm SN} t^2}{\rho_{\rm bk}}\right)^{1/5} \tag{A6}$$

where t is the time after the explosion and $\rho_{\rm bk}$ is the ambient gas density, scaling as $(\Omega_{\rm b}/\Omega_{\rm m})M_{\rm h}/R_{\rm vir}^3$. The velocity of the shell $v_{\rm sh}$ in the Sedov-Taylor approximation is given by $2/5 R_{\rm sh}/t$. Under these conditions, $v_{\rm sh}(R_{\rm vir})$ can be easily inferred. At the time $R_{\rm sh} = R_{\rm vir}$ the kinetic energy is

$$K_{\rm SN} = 0.67 \frac{\Omega_{\rm m}}{\Omega_{\rm b}} \frac{M_{\rm sh}}{M_{\rm h}} f_w \mathcal{E}_{\rm SN}. \tag{A7}$$

To compute $M_{\rm sh}$ for a given halo we recure to energy conservation leading to

$$\left(1 - 0.67\frac{\Omega_{\rm m}}{\Omega_{\rm b}}\frac{M_{\rm sh}}{M_{\rm h}}\right) f_w \mathcal{E}_{\rm SN} = \frac{GM_{\rm h}M_{\rm sh}}{R_{\rm vir}} \left[2\left(1 + \frac{\Omega_{\rm b}}{\Omega_{\rm m}}\right) - \frac{M_{\rm sh}}{M_{\rm h}}\right]. \tag{A8}$$

We note that $M_{\rm sh}/M_{\rm h}$ is always much less than $2\,(1 + \Omega_{\rm b}/\Omega_{\rm m})$. Negletting the term $M_{\rm sh}/M_{\rm h}$ in parentesis on the right side of the equation the outflow mass of the first single bubble is given by

$$M_{\rm sh} = \frac{f_w \mathcal{E}_{\rm SN}}{2\,(1 + \Omega_{\rm b}/\Omega_{\rm m})\, GM_{\rm h}/R_{\rm vir} + \frac{1}{2}v_{\rm sh}^2}. \tag{A9}$$

We assume that an outflow develops only when $v_{\rm sh} > v_{\rm esc}$. Otherwise $M_{\rm sh} = 0$.

Massive halos are not compleately evacuated after this first SN episode. Further star formation is often allowed and to account for subsequent SN esplosion episodes we compute

[7] Note that the actual gas density profile at the moment of SN explosions would be quite different from the initial one. Differences would arise both from the fact that the gas needs to cool down in order to form stars, and from the radiative feedback of stars during their lifetimes.

the total number of exploding SNae $N_{\rm SN}$ between time t_1 and t_2

$$N_{\rm SN} = \int_{t_1}^{t_2} \nu_{\rm SN} \left(\epsilon_{\rm SF} \dot{M}_{\rm inf} + \dot{M}_{*,\rm d} \right) {\rm d}s. \quad \text{(A10)}$$

We define $M_{\rm sh,s}$ as the contribution of a single esplosion (i.e. equation A9 with $\mathcal{E}_{\rm SN} = E_{\rm SN}$). An Outflow develops only if it injects sufficient energy so that $v_{\rm sh} > v_{\rm esc}$. This requires a minimum energy in a single bubble, i.e. a minimum number of SNae. For a given $\dot{M}_*$, we calculate the expected number of SNae on a timescale of the order of their progenitor lifetimes (i.e. 3 Myr). If the resulting $v_{\rm sh}$ is greater than the escape velocity from the halo, outflows are allowed and

$$\dot{M}_{\rm sh} = M_{\rm sh,s} \frac{{\rm d}N_{\rm SN}}{{\rm d}t} = \frac{f_w \nu E_{\rm SN} \left(\epsilon_{\rm SF} \dot{M}_{\rm inf} + \dot{M}_{*,\rm d} \right)}{2 \left(1 + \frac{\Omega_{\rm b}}{\Omega_{\rm m}} \right) \frac{G M_{\rm h}}{R_{\rm vir}} + \frac{1}{2} v_{\rm sh}^2}. \quad \text{(A11)}$$

Otherwise $\dot{M}_{\rm sh} = 0$.

References

Abel, T., Bryan, G. L., & Norman, M. L. 2000, ApJ, 540, 39–44.
Balcells, M., Graham, A. W., & Peletier, R. F. 2007, ApJ, 665, 1104
Barkana, R., & Loeb, A. 2001, PhR, 349, 125
Begelman, M. C., Volonteri, M., & Rees, M. J. 2006, MNRAS, 370, 289
Böker, T., Sarzi, M., McLaughlin, D. E., van der Marel, R. P., Rix, H.-W., Ho, L. C., & Shields, J. C. 2004, AJ, 127, 105
Bromm, V., & Loeb, A. 2003, Nature, 425, 812
Bromm, V., Coppi, P. S., & Larson, R. B. 1999, ApJL, 527, L5–L8.
Bromm, V., Ferrara, A., Coppi, P. S., & Larson, R. B. 2001, MNRAS, 328, 969
Capuzzo-Dolcetta, R., & Miocchi, P. 2008, MNRAS, 388, L69
Clark, P. C., Glover, S. C. O., & Klessen, R. S. 2008, ApJ, 672, 757
Cole, S., Lacey, C. G., Baugh, C. M., & Frenk, C. S. 2000, MNRAS, 319, 168
Côté, P., et al. 2006, ApJS, 165, 57
Devecchi, B., & Volonteri, M. 2009, ApJ, 694, 302
Dunkley, J., et al. 2008, ArXiv e-prints, 803, arXiv:0803.0586
Eisenstein, D. J., & Loeb, A. 1995, ApJ, 443, 11
Elmegreen, B. G., & Efremov, Y. N. 1997, ApJ, 480, 235
Ferrara, A., Pettini, M., & Shchekinov, Y. 2000, MNRAS, 319, 539
Ferrarese, L., et al. 2006, ApJ, 644, L21
Freese, K., Bodenheimer, P., Spolyar, D., & Gondolo, P. 2008, ArXiv e-prints, 806, arXiv:0806.0617
Freitag, M., Gürkan, M. A., & Rasio, F. A. 2006, MNRAS, 368, 141
Freitag, M., Rasio, F. A., & Baumgardt, H. 2006, MNRAS, 368, 121
Gammie, C. F. 2001, ApJ, 553, 174
Glebbeek, E., Gaburov, E., de Mink, S. E., Pols, O. R., & Portegies Zwart, S. F. 2009, A&A, 497, 255
Graham, A. W., & Spitler, L. R. 2009, MNRAS, 397, 2148
Greif, T. H., Johnson, J. L., Bromm, V., & Klessen, R. S. 2007, ApJ, 670, 1
Gürkan, M. A., Freitag, M., & Rasio, F. A. 2004, ApJ, 604, 632
Haehnelt, M. G. & Rees, M. J., MNRAS 263, 168–178.
Heger, A., Fryer, C. L., Woosley, S. E., Langer, N., & Hartmann, D. H. 2003, ApJ, 591, 288
Iocco, F., Bressan, A., Ripamonti, E., Schneider, R., Ferrara, A., & Marigo, P. 2008, MNRAS, 390, 1655
Klessen, R. S., Krumholz, M. R., & Heitsch, F. 2009, arXiv:0906.4452
Kennicutt, R. C., Jr. 1998, ApJ, 498, 541
Koushiappas, S. M., Bullock, J. S., & Dekel, A. 2004, MNRAS, 354, 292
Kulkarni, V. P., Fall, S. M., Lauroesch, J. T., York, D. G., Welty, D. E., Khare, P., & Truran, J. W. 2005, Apj, 618, 68
Li, L.-X. 2007, ArXiv e-prints, 710, arXiv:0710.3587
Li, Y., Haiman, Z., & Mac Low, M.-M. 2007, ApJ, 663, 61
Lin, D. N. C., & Pringle, J. E. 1987, MNRAS, 225, 607
Lodato, G. 2007, Nuovo Cimento Rivista Serie, 30, 293
Lodato, G., & Natarajan, P. 2006, MNRAS, 371, 1813
Loeb, A., & Rasio, F. A. 1994, ApJ, 432, 52
Lotz, J. M., Telford, R., Ferguson, H. C., Miller, B. W., Stiavelli, M., & Mack, J. 2001, ApJ, 552, 572
Madau, P., & Rees, M. J. 2001, ApJ, 551, L27
Milosavljević, M. 2004, ApJ, 605, L13
Mineshige, S., & Umemura, M. 1997, ApJ, 480, 167
Mo, H. J., Mao, S., & White, S. D. M. 1998, MNRAS, 295, 319
Monaco, P., Theuns, T., Taffoni, G., Governato, F., Quinn, T., & Stadel, J. 2002, ApJ, 564, 8
Monaco, P., Theuns, T., & Taffoni, G. 2002, MNRAS, 331, 587
Mori, M., Ferrara, A., & Madau, P. 2002, ApJ, 571, 40
Omukai, K., & Palla, F. 2003, ApJ, 589, 677
Omukai, K., Schneider, R., & Haiman, Z. 2008, ArXiv e-prints, 804, arXiv:0804.3141
Portegies Zwart, S. F., Makino, J., McMillan, S. L. W., & Hut, P. 1999, A&A, 348, 117
Portegies Zwart, S. F., Baumgardt, H., Hut, P., Makino, J., & McMillan, S. L. W. 2004, Nature, 428, 724
Portegies Zwart, S. F., & McMillan, S. L. W. 2002, ApJ, 576, 899
Prochaska, J. X., Chen, H.-W., Dessauges-Zavadsky, M., & Bloom, J. S. 2007, Apj, 666, 267
Prochaska, J. X., Gawiser, E., Wolfe, A. M., Castro, S., & Djorgovski, S. G. 2003, Apj, 595, L
Rees, M. J. 1984, ARA&A, 22, 471
Rossa, J., van der Marel, R. P., Böker, T., Gerssen, J., Ho, L. C., Rix, H.-W., Shields, J. C., & Walcher, C.-J. 2006, AJ, 132, 1074
Santoro, F., & Shull, J. M. 2006, ApJ, 643, 26
Savaglio, S. 2006, New Journal of Physics, 8, 195
Savaglio, S., et al. 2005, Apj, 635, 260
Scannapieco, E., Schneider, R., & Ferrara, A. 2003, ApJ, 589, 35
Schneider, R., Omukai, K., Inoue, A. K., & Ferrara, A. 2006, MNRAS, 369, 1437

Seth, A., Agüeros, M., Lee, D., & Basu-Zych, A. 2008, ApJ, 678, 116
Sheth, R. K., & Tormen, G. 1999, MNRAS, 308, 119
Sutherland, R. S., & Dopita, M. A. 1993, ApJS, 88, 253
Toomre, A. 1964, ApJ, 139, 1217
Tornatore, L., Ferrara, A., & Schneider, R. 2007, MNRAS, 382, 945
Tremaine, S. D., Ostriker, J. P., & Spitzer, L., Jr. 1975, ApJ, 196, 407
Volonteri, M., Haardt, F., & Madau, P. 2003, ApJ, 582, 559
Volonteri, M., Lodato, G., & Natarajan, P. 2008, MNRAS, 383, 1079
Walcher, C. J., Böker, T., Charlot, S., Ho, L. C., Rix, H.-W., Rossa, J., Shields, J. C., & van der Marel, R. P. 2006, ApJ, 649, 692
Wehner, E. H., & Harris, W. E. 2006, ApJ, 644, L17
White, S. D. M., & Rees, M. J. 1978, MNRAS, 183, 341
Woosley, S. E., & Weaver, T. A. 1995, ApJS, 101, 181